

Experimental study on mechanical performances of lattice steel reinforced concrete inner frame with irregular section columns

Jiayang Xue^{*1}, Liang Gao¹, Zuqiang Liu¹, Hongtie Zhao¹ and Zongping Chen²

¹ College of Civil Engineering, Xi'an University of Architecture and Technology, Xi'an, P.R. China

² College of Civil and Architectural Engineering, Guangxi University, Nanning, P.R. China

(Received February 12, 2013, Revised July 25, 2013, Accepted October 23, 2013)

Abstract. Based on the test on a 1/2.5-scaled model of a two-bay and three-story inner frame composed of reinforced concrete beams and lattice steel reinforced concrete (SRC) irregular section columns under low cyclic reversed loading, the failure process and the features of the frame were observed. The subsequence of plastic hinges of the structure, the load-displacement hysteresis loops and the skeleton curve, load bearing capacity, inter-story drift ratio, ductility, energy dissipation and stiffness degradation were analyzed. The results show that the lattice SRC inner frame is a typical strong column-weak beam structure. The hysteresis loops are spindle-shaped, and the stiffness degradation is insignificant. The elastic-plastic inter-story deformation capacity is high. Compared with the reinforced concrete frame with irregular section columns, the ductility and energy dissipation of the structure are better. The conclusions can be referred to for seismic design of this new kind of structure.

Keywords: lattice steel; steel reinforced concrete (SRC); inner frame with irregular section columns; quasi-static test; mechanical performance

1. Introduction

An irregular section column is the column with irregular sectional shape, such as L, T, cross and Z shape. The width remains constant between columns and infilled walls, which makes fully use of available space, and the aesthetic appearance of structure is improved. Since it possesses the aforementioned advantages, the reinforced concrete (RC) irregular section column is firstly studied and widely used in the practical engineering projects in China. However, RC irregular section columns have some obvious drawbacks, such as low bearing capacity, weak seismic performance, etc. (Tsao 1993, Balaji 2001, Cao *et al.* 2007). In order to overcome the defects of RC irregular section columns, structural system with steel reinforced concrete (SRC) irregular section columns is proposed (Chen *et al.* 2007). The SRC irregular section column is the combination of irregular section and SRC column, which has good aesthetic appearance, high load bearing capacity and good seismic performance, and has become a popular research topic in many scientific institutes (Kim 2011, Ma 2011, Pecce 2012). At present, researches about this structural system mainly focus on the component of irregular section columns and column-beam joints (Xue

*Corresponding author, Professor, Ph.D., E-mail: jiayang_xue@163.com

et al. 2011). However, few have been done on the integral structural system. In 2007, a pseudo-static test on a 1/2-scaled model of a one-bay and two-story frame composed of RC beams and T-shaped section columns was conducted by researchers in Guangxi University (Yang and Zhang 2009). Restricted by the form of the specimen, the experiment could not reveal the mechanical performance of the typical SRC frame with irregular section column comprehensively. This paper presents the failure process and the features, and analyzed the mechanical performances of the structure based on the experiment on a 1/2.5-scaled model of a two-bay and three-story inner frame composed of reinforced concrete beams and lattice SRC irregular section columns under low cyclic reversed loading. This work attempts to be helpful for popularizing the new structural system construction in high seismic zone.

2. Test outline

2.1 Test specimen design and fabrication

According to the seismic intensity of degree 8, a 1/2.5-scaled specimen of a lattice SRC inner frame with irregular section columns was designed, which consisted of reinforced concrete beams and lattice SRC irregular section columns. The bottom level, the intermediate level, and the top level were selected as the first-, the second- and the third- story of the prototype respectively for the analysis. The geometry, steel and reinforcement layout of the test specimen are shown in Fig. 1.

The test specimen was cast using fine aggregate commercial concrete, and the cubic concrete compressive strength measured at the 28th day was 30.35MPa. Grade Q235B steel was used as the steel skeleton in columns. The T-shaped steel was welded by using steel plates in relevant specification in form of double-sided fillet welt. Flat steel with 20 mm in width and 8mm in thickness was used as the horizontal and cross diagonal web members to form the steel truss (Fig. 2). The average steel reinforcement ratio of the edge column and inner column was 5.76% and 5.12%, respectively. $\phi 8$ bars were used as the longitudinal steel bars in columns, and the reinforcement ratio was 0.85%. $\phi 12$ bars were used as the longitudinal steel bars in first- and second-story beams, the reinforced bars were placed symmetrically and the reinforcement ratio

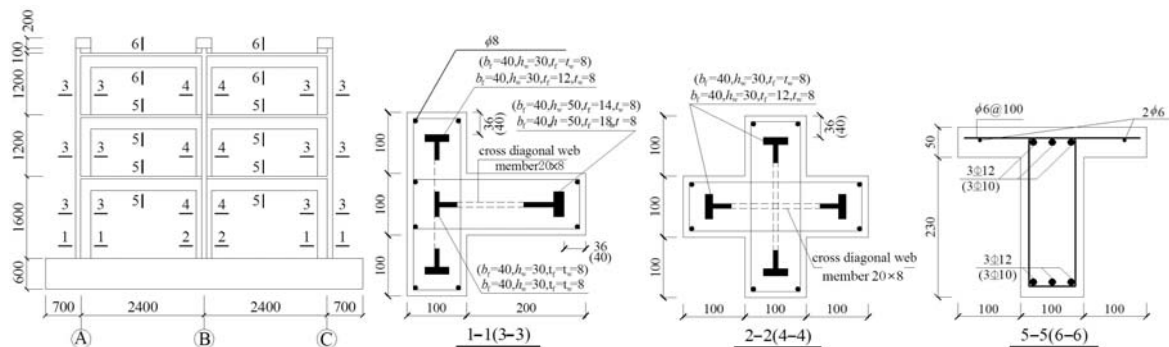


Fig. 1 Geometry and steel layout of the test specimen

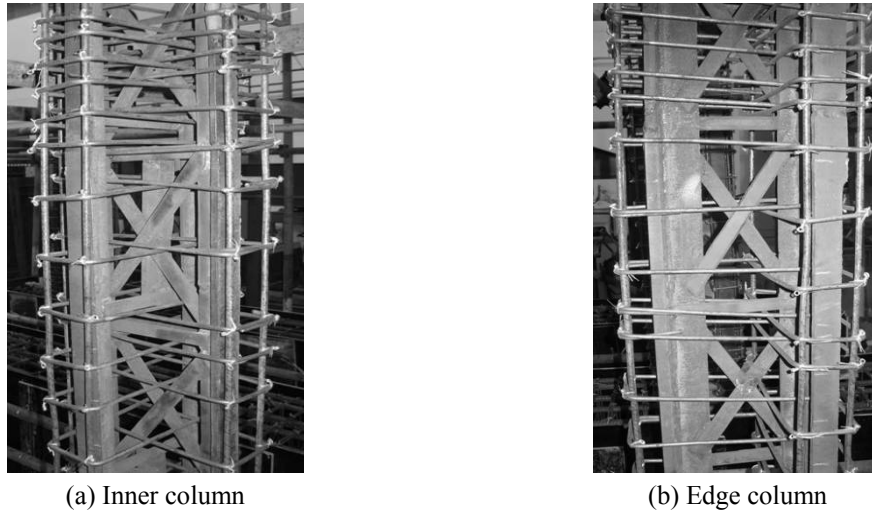


Fig. 2 Steel skeleton

Table 1 Properties of steel bars and steel plates

Material	Diameter (Plate thickness)	Yield strength f_y /MPa	Ultimate strength f_u /MPa	Elastic modulus E_s /MPa
Steel bars	$\phi 6$	302.31	443.68	2.24×10^5
	$\phi 8$	320.74	472.68	2.36×10^5
	$\phi 10$	439.04	653.98	1.95×10^5
	$\phi 12$	406.33	597.34	1.92×10^5
Steel plates	8 mm	323.76	459.92	1.93×10^5
	12 mm	471.53	605.71	2.10×10^5
	14 mm	316.37	471.91	2.11×10^5
	18 mm	302.86	465.05	1.72×10^5

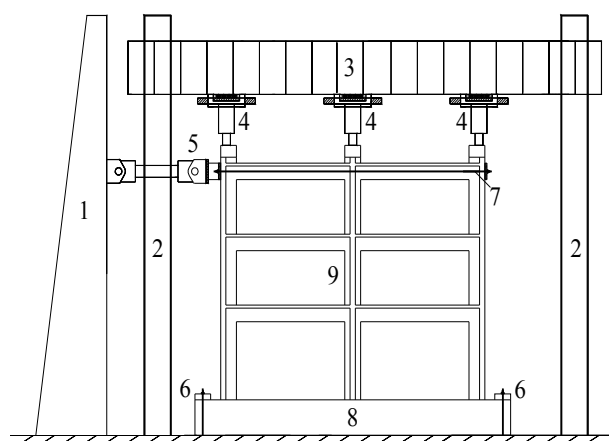
was 1.33%, $\phi 10$ bars were used as the longitudinal steel bars in the third-story beams, the reinforced bars were arranged symmetrically and the reinforcement ratio was 0.92%. $\phi 6$ bars were used as the stirrups in both the columns and the beams, and the stirrup ratio of the columns and the beams was 2.27% and 0.71%, respectively. In the 300 mm range of each column end, 400 mm range of each beam end and the whole joints zone, the stirrups were arranged at intervals of 40 mm, and in other parts of the test specimen, the stirrups were arranged at intervals of 80 mm. Properties of steel bars and steel plates are shown in Table 1.

2.2 Test procedure

The load was applied by three hydraulic jacks on the top of each column of the test specimen. 255.6 kN force was loaded axially on top of each edge column, and 511.2 kN force was loaded

axially at the top of the inner column, the design value of axial compression ratio of the edge columns and the inner column is 0.2 and 0.4, respectively. The values of vertical load remain constant during the whole loading process. The lateral low-cycle reversed load was applied at the top beam end by the MTS electro-hydraulic servosystem. Horizontal movement of the footing during loading was restrained by the friction force between the footing and the floor. The pressure was applied to the footing by two steel blocks, which were connected to the test floor by 4 post-tensioned high strength threaded rods. The footing rotations were also restrained by the two steel blocks. Strain gages were mounted at critical positions on the steel, longitudinal steel bars and stirrups to measure the strain history during the test. The first critical section was the beam end section (Nie *et al.* 2004, Ju *et al.* 2009), which was 100 mm away from the nearest surface of the columns. The second critical section was the column end section (Karimi *et al.* 2012), which was 100 mm away from the nearest surface of the beam-column joints. The third one was the midst of beam-column joints (Kawano *et al.* 2012). Unidirectional strain gages were attached on top and bottom flanges at these sections. All the data was collected by TDS-602 static data acquisition instrument. The test setup is shown in Fig. 3.

A load-displacement hybrid control program was applied, in which the lateral loading sequence was controlled by force for the initial loading cycles till the yielding initiation of the test specimen was observed. This observation was accomplished by monitoring the reaction forces of the MTS horizontal actuator. From 30 kN, every load level was applied for one cycle in an increment of 30 kN. When the test specimen started yielding, the loading sequence was controlled by displacement. On the basis of the yield displacement, the target displacements for the cyclic loading were set as the multiple of the yield displacement (Δ_y), the cyclic loadings were repeated three times at each target displacement. Loading was terminated until the reaction force descended to about 85% of the maximum value. The loading process is shown in Fig. 4. During the test, the load/displacement was kept constant at several loading stage so that the data could be recorded by the acquisition instrument, cracks could be marked, crack width could be measured, and pictures could be taken.



1 reaction wall; 2 reaction steel frame; 3 reaction girder; 4 vertical actuator;
5 1000kN horizontal actuator; 6 tie bolt; 7 horizontal braces; 8 footing; 9 test specimen

Fig. 3 Test setup

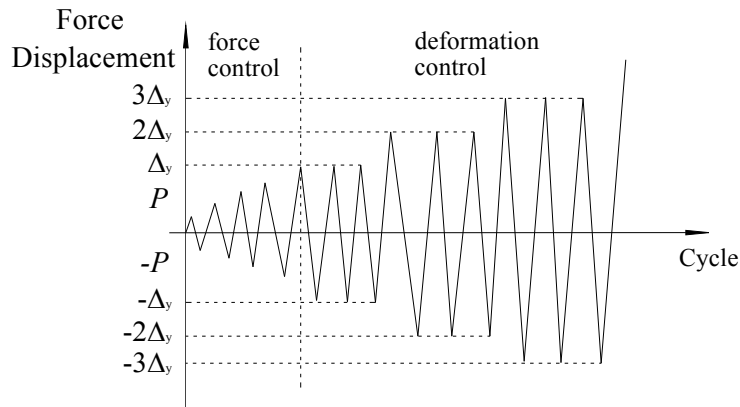


Fig. 4 Loading control process

3. Test phenomenon

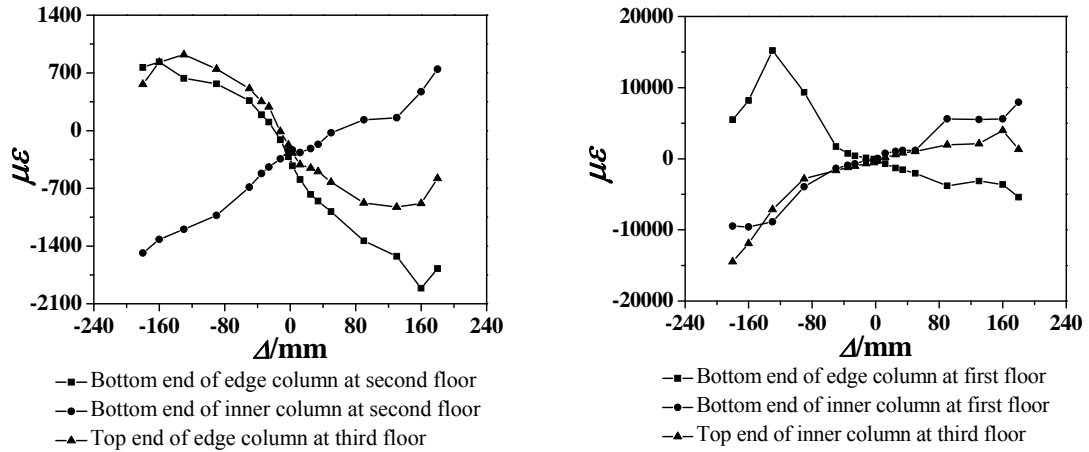
3.1 The main failure modes

3.1.1 Columns

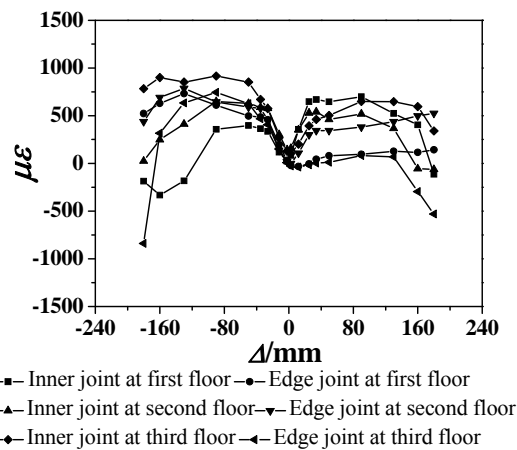
Under a lateral loading of 90 kN, horizontal cracks occurred at each bottom end of the first-story column web. As the lateral loading increased, horizontal cracks formed at the flange of the first-story column bottom ends. When the lateral displacement of the top beam reached 90 mm and was repeated 3 times (the corresponding horizontal load was 242 kN), cover concrete spalling developed at the web of the first- and the third-story column bottom ends. With further increment of top beam lateral displacement, concrete crushed and dropped at column bottom and column webs of each story, vertical cracks formed at the position of stirrups, and longitudinal steel bars and stirrups were exposed. When the displacement of the top beam reached 180 mm and was repeated 3 times (the corresponding horizontal load was 168 kN), a great number of longitudinal steel bars and stirrups were exposed at the web of column bottom ends, but few concrete at column flange was crushed for the first-story columns. For the second-story columns, longitudinal steel bars were exposed at the inner column bottom end. For the third-story columns, concrete was crushed and dropped more, and the longitudinal steel bars at the web of column bottom ends were compressed to be unstable. From the strain distribution of the column steel it can also be concluded that no plastic hinges developed at most column ends (Fig. 5(a)), except for the ends at the first story column and the upper end of the inner column at the third story (Fig. 5(b)).

3.1.2 Beams

Under a horizontal loading of 30 kN, flexural cracks occurred at each first-story beam end. As the lateral loading increasing, more flexural cracks were observed occurring and developing. Under a loading of 60 kN, flexural cracks occurred at each second- and third-story beam end. Under a loading of 150 kN, few diagonal shear cracks occurred at each first- and second-story beam end. Under a loading of 210 kN, the main flexural cracks formed at the first- and second-story beam ends, and the width of the cracks was about 1~2 mm. When the displacement



(a) Steel strain at non-plastic hinge field of column (b) Steel strain at plastic hinge field of column



(c) Strain of horizontal web steel at panel zone

Fig. 5 Strain of the shape steels

of the top beam reached 90 mm and was repeated 3 times (the corresponding horizontal load was 242 kN), concrete crushed and dropped at the bottom side of the first and second-story beam ends, stirrups at the flange of the beam end were exposed, and the main flexural cracks formed at the third-story beam ends. When the displacement of the top beam reached 160 mm and was repeated 3 times (the corresponding horizontal load was 203 kN), the concrete dropping from the beam base ends and flanges increased, concrete at the top of the flange plate was crushed, and the longitudinal steel bars at first-story beam were exposed. When the displacement of the top beam reached 180 mm and was repeated 3 times (the corresponding horizontal load was 168 kN), a large amount of concrete at each beam end dropped, some longitudinal steel bars at bottom side of beam end fractured, and the concrete crushing at the top of the flange plate grew continuously.



(a) The edge joint at third-story



(b) The inner joint at second-story



(c) The breaking of longitudinal steel bars at the base of beam end



(d) The edge column bottom end of first-story



(e) Test specimen after failure

Fig. 6 Failure modes of test specimen

3.3 Beams-column joints

Under a horizontal loading of 90 kN, the cracks at beam end extended to the marginal area of beam-column joints. Under a loading of 150 kN, tiny diagonal shear cracks occurred at the middle area of each beam-column joint. When the loading sequence was controlled by displacement, cover concrete spalling developed at each beam-column joints. When the displacement of the top beam reached 180 mm and repeated for 3 times (the corresponding horizontal load was 168 kN), concrete spalling of each story grew continuously, the stirrups and longitudinal steel bars were exposed, but the horizontal web steel did not yield at last (Fig. 5(c)).

Overall, the failure of the upper part of the test specimen was more severe than that of the lower part. The damage initiated at each beam end firstly and the damage was the most severe. The cracks mainly spreaded in the 1/3 area of each beam end, and plastic hinges developed at all the beam ends. For the columns, damage was concentrated at the bottom ends, and the damage was not as severe as that of the beams. The plastic hinges developed at the first-story column bottom ends and the top end of the third-story inner column. Damage happened slightly and finally at the beam-column joints. It shows that, the failure mechanism of the test specimen was the beam-hinged mechanism, satisfying the seismic design principle of “strong column and weak beam”

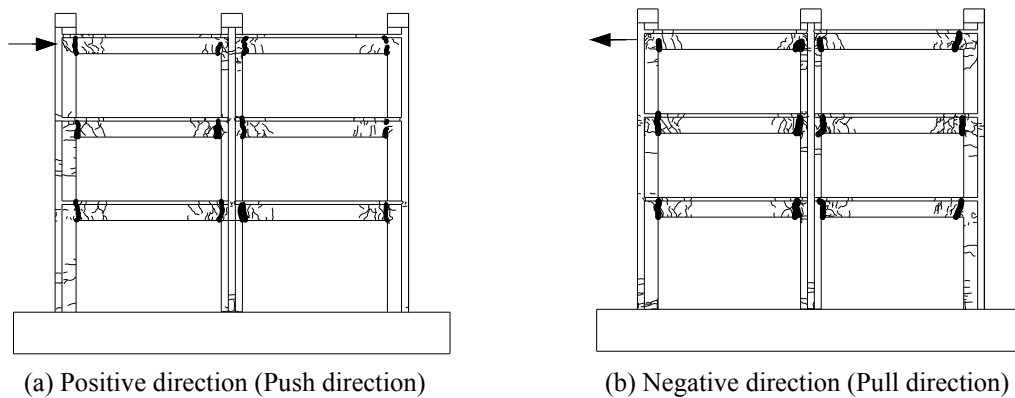


Fig. 7 Cracking of test specimen

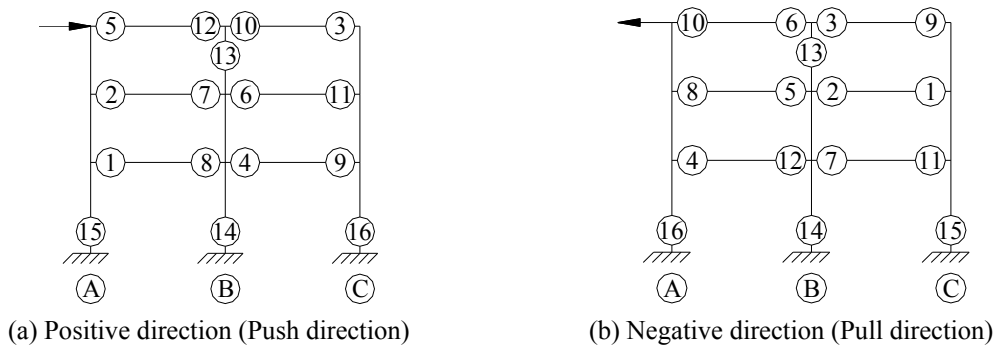


Fig. 8 Subsequence of plastic hinges of test specimen

(Tago *et al.* 2012). The failure mode of the test specimen is shown in Fig. 6, the ultimate cracking pattern is shown in Fig. 7, in which the positive and negative direction represents the push and pull direction of loading, respectively. The subsequence of plastic hinges of the test specimen is shown in Fig. 8.

3.2 Hysteresis loops and skeleton curves

The hysteresis loops and skeleton curves reflect the relationship between the load and the deformation of the whole structure comprehensively. They are the macroscopic reflection of the seismic performance of the structure and the main basis of the elasto-plastic dynamic response analysis. The lateral load-displacement hysteresis loops and skeleton curve obtained from the test are shown in Figs. 9 and 10, respectively. The figures suggest that

- (1) At the early stage of loading, the area of the hysteresis loops was very small. There was a linear relationship between the lateral force and the displacement. Stiffness variation was insignificant, and the residual deformation was negligible.
- (2) With the increment of lateral load, the hysteresis loops became plumper. Obvious residual deformation was formed, and the test specimen was in the nonlinear stage.
- (3) After the test specimen yielded, the lateral load of the specimen gradually increased with the increasing of the lateral displacement, till the peak load was reached. The bearing capacity began to descend. The area of the hysteresis loops continued enlarging. Under the cyclic loading, the damage on the test specimen accumulated gradually, and the stiffness of the structure degraded slowly.
- (4) The hysteresis loops in positive and negative direction were symmetric; the hysteresis loops were in spindle shape, and then transformed into bow shape, indicating that the test specimen had a good seismic performance.
- (5) During the whole loading process, the test specimen exhibited large initial stiffness, load bearing capacity, and deformation capacity. The skeleton curve of the test specimen possessed a long descent trajectory, and the descending branch was gentle. This indicated that the structure had good ductility and energy dissipation capacity.

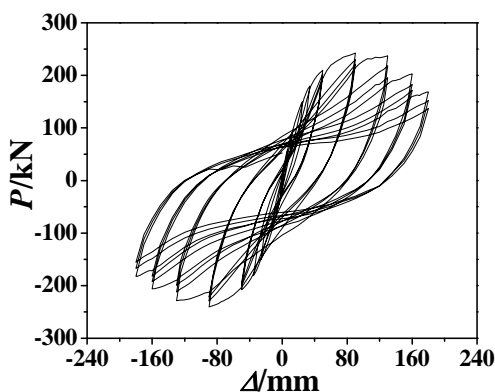


Fig. 9 P - Δ hysteresis loops of test specimen

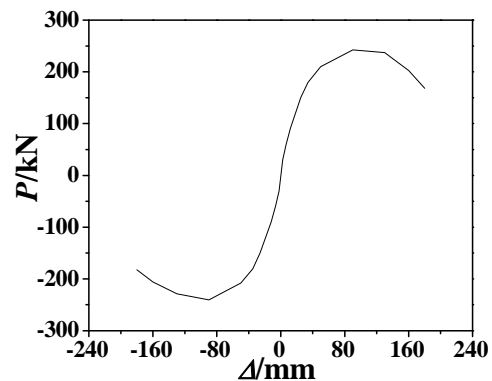


Fig. 10 P - Δ skeleton curve of test specimen

4. Mechanical performance analysis

4.1 Bearing capacity and inter-story drift ratio

The bearing capacity and inter-story drift obtained from the test are shown in Table 2. P_y stands for the yield load, which was confirmed with the method of universal yield moment (Lubliner 2006). P_p stands for the peak load, and P_f stands for the failure load. Δ_y , Δ_p and Δ_f are the displacements correspond to the load P_y , P_p and P_f , respectively. θ_y , θ_p and θ_f are the inter-story drift ratio respectively correspond to the load P_y , P_p and P_f . The inter-story drift was defined as $\theta_i = \Delta_i/H$, where Δ_i stands for the inter-story displacement, H stands for the story height.

Table 2 shows that the bearing capacities in positive and negative direction of the test specimen were approximately the same, and the ratio of yield to peak load was about 77.2%. Each inter-story displacement in positive and negative direction was approximately the same, indicating that the test specimen had uniform vertical stiffness, and there was no obvious weak story. The integral drift ratio of the test specimen was 1/24, much larger than the limit value specified by the Chinese Seismic Design Code. Each inter-story drift ratio was also greater than the limit value specified by the code, in which the limit equals to 1/50. This indicates that the test specimen has a good elasto-plastic deformation capacity.

4.2 Energy dissipation capacity

4.2.1 Displacement ductility coefficient

The displacement ductility coefficient is an important index reflecting the seismic performance of structures (Chen 2005). The displacement ductility coefficient was defined as $\mu = \Delta_f/\Delta_y$, where Δ_f stands for the failure displacement, Δ_y stands for the yield displacement. The displacement ductility coefficients were shown in Table 3. It is shown that the positive and negative inter-story displacement ductility coefficients ranged from 4.1 to 4.4, the integral displacement ductility coefficients in positive and negative directions were 4.3 and 4.6, respectively. Compared with the reinforced concrete frame with irregular section columns whose ductility coefficients is about 3.6 (Wang *et al.* 2007), the ductility of the structure are better, indicating that the lattice SRC frame with irregular section columns has excellent deformation capacity.

Table 2 Experimental results at main loading stages

Position	Loading direction	Yield point			Peak point			Failure point			μ
		P_y/kN	Δ_y/mm	θ_y	P_p/kN	Δ_p/mm	θ_p	P_f/kN	Δ_f/mm	θ_f	
Integrity	Positive	187.1	38.8	1/103	242.3	94.4	1/42	206.0	167.3	1/24	4.3
	Negative	185.9	36.2	1/111	240.3	90.1	1/44	204.3	166.9	1/24	4.6
First-story	Positive	187.1	13.6	1/118	242.3	33.6	1/48	206.0	60.0	1/27	4.4
	Negative	185.9	9.3	1/167	240.3	21.7	1/74	204.3	38.7	1/41	4.2
Second-story	Positive	187.1	12.2	1/98	242.3	30.3	1/40	206.0	50.3	1/24	4.1
	Negative	185.9	11.6	1/103	240.3	27.8	1/43	204.3	50.6	1/24	4.4
Third-story	Positive	187.1	13.0	1/92	242.3	30.5	1/39	206.0	57.0	1/21	4.4
	Negative	185.9	15.3	1/78	240.3	40.6	1/30	204.3	67.6	1/18	4.4

Table 3 Ductility coefficients

Position	Integrity		First-story		Second-story		Third-story	
	Positive	Negative	Positive	Negative	Positive	Negative	Positive	Negative
μ	4.3	4.6	4.4	4.2	4.1	4.4	4.4	4.4

4.2.2 Equivalent viscous damping coefficient

Equivalent viscous damping coefficient h_e is an important index reflecting the energy dissipation capacity of the structure. By analyzing the hysteresis loops of the test specimen under low cyclic reversed loading, the degree of energy dissipation under different loading level can be investigated. The equivalent viscous damping coefficient can be written as follows

$$h_e = \frac{1}{2\pi} \cdot \frac{S_{(ABCD A)}}{S_{(OBE+ODF)}} \tag{1}$$

in which $S_{(ABCD A)}$ represents the area of the hysteresis loop ABCDA, $S_{(OBE+ODF)}$ represents the area of the triangles OBE and ODF, as indicated in Fig. 11. The calculated results of the test specimen are shown in Table 4, in which h_{ey} , h_{ep} and h_{ef} stand for the yield, peak and failure equivalent viscous damping coefficient, respectively. The relevant research papers show that, the equivalent viscous damping coefficient of frame structure ranges from 0.05 to 0.25 (Wang *et al.* 2008). The equivalent viscous damping coefficient of the test specimen falls right in the range. Compared with the reinforced concrete frame with irregular section columns whose h_{ey} , h_{ep} and h_{ef} is 0.069, 0.132 and 0.160 respectively (Wang *et al.* 2008), the energy dissipation capacity of the lattice SRC frame is better.

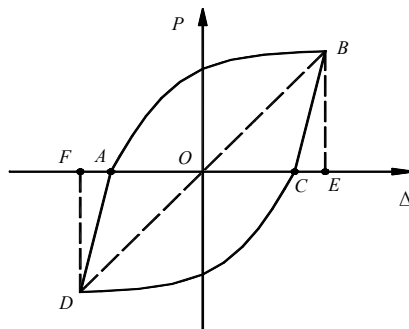


Fig. 11 The calculation of equivalent viscous damping coefficient

Table 4 Equivalent viscous damping coefficients of specimen

Test specimen	h_e		
	h_{ey}	h_{ep}	h_{ef}
	0.078	0.172	0.212

Table 5 Coefficient of stiffness degradation

λ_i	Integrity		First-story		Second-story		Third-story	
	Positive	Negative	Positive	Negative	Positive	Negative	Positive	Negative
λ_{yi}	1.000	1.000	1.000	1.000	1.000	1.000	1.000	1.000
	0.964	0.958	0.950	0.968	0.967	0.962	0.976	0.949
	0.939	0.933	0.922	0.947	0.942	0.938	0.953	0.922
λ_{pi}	1.000	1.000	1.000	1.000	1.000	1.000	1.000	1.000
	0.949	0.952	0.914	0.974	0.960	0.953	0.979	0.941
	0.913	0.918	0.872	0.954	0.925	0.919	0.949	0.900
λ_{fi}	1.000	1.000	1.000	1.000	1.000	1.000	1.000	1.000
	0.901	0.930	0.901	0.938	0.907	0.932	0.895	0.925
	0.848	0.879	0.856	0.886	0.852	0.883	0.835	0.873

*Note : λ_{yi} , λ_{pi} and λ_{fi} stands for the yield, peak and failure coefficient of stiffness degradation, respectively

4.3 Stiffness

The stiffness degradation reflects the degradation of the resistance of lateral collapse. The stiffness of the test specimen under low cyclic reversed loading can be expressed in secant stiffness. Secant stiffness is the ratio of peak load in every load level and the associated displacements in positive and negative direction. The integral and inter-story stiffness degradation coefficient λ_i of the test specimen under different loading levels denoting the ratio of the stiffness in the i -th time and the stiffness in the first time in the same displacement-controlled cycle is shown in Table 5. It shows that the stiffness degradation of the test specimen is not obvious under the same displacement-controlled cycle. With the increment of displacement in different loading levels, the stiffness degradation gets more severe. The inter-story stiffness degradation in positive and negative direction is closely approximated.

The inter-story stiffness degradation is relevant to the occurrence and development of cracks in different parts of the test specimen in the loading process. At first, cracks occurred at the beam ends, the corresponding lateral load was about 30 kN, which was about 12.4% of the lateral peak load. Then cracks occurred at the column ends, the corresponding lateral load was about 90 kN, 37.1% of the lateral peak load. When the lateral load was 150 kN, cracks occurred in the beam-column joints, and the ratio of 150 kN to lateral peak load was 61.9%. When the main flexural cracks formed at the beam ends, the test specimen was observed to yield, and the corresponding lateral load was about 190 kN, 79.2% of the lateral peak load. Fig. 12 shows the relationship between inter-story stiffness degradation and the change of inter-story drift ratio, K_i stands for the inter-story stiffness under different loading level, K_{ei} stands for the initial elastic inter-story stiffness, θ stands for the inter-story drift ratio.

The integral and inter-story stiffness degradations of the test specimen under different loading levels are provided in Fig. 13. Fig. 13(a) shows that the initial stiffness in positive and negative direction of the test specimen was similar, and the extent of stiffness degradation was symmetric. Before the test specimen yielded, a lot of concrete cracks occurred which led to fast stiffness

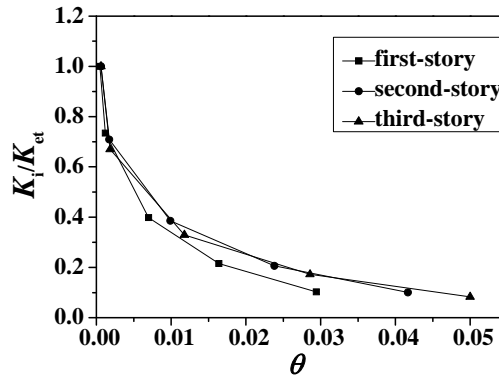


Fig. 12 The relationship between inter-story drift ratio and the stiffness degradation

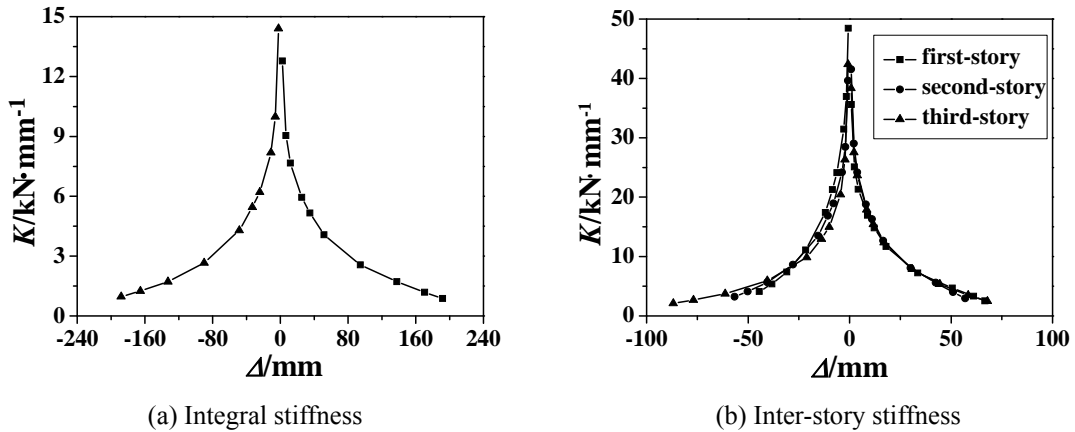


Fig. 13 Curves of stiffness degradation

degradation. With the development of plastic deformation, the stiffness degradation slowed down gradually. Fig. 13(b) shows that the inter-story stiffness degradation follows the same pattern with the integral stiffness degradation. Although the first-story height is larger than the other two stories, the first-story column ends have been strengthened. Therefore, the test specimen has uniform vertical stiffness in the entire loading process.

5. Conclusions

An experimental study was performed to investigate the structural performance of a lattice SRC inner frame with irregular section columns. The structural system was subjected to low-cycle reversed loading. The findings from the experimental study are summarized as follows:

- (1) During the loading process, plastic hinges firstly occurred at all the beam ends, and then occurred at the first-story column ends. The failure mechanism of the test specimen is the

beam-hinged mechanism, satisfying the seismic design principle of “strong column and weak beam”.

- (2) The hysteresis loops of the test specimen were in a spindle-shape, the stiffness degradation showed a fast to slow pattern. It was shown that the stiffness degradation of the test specimen was not obvious under the same displacement-controlled cycle. With the increase of the displacement in different loading levels, the stiffness degradation became more and more serious, and the extent of inter-story stiffness degradation in positive and negative direction was approximated closely.
- (3) The test specimen had good deformation capacity. The ultimate inter-story drift ratio was over 1/50, and the ultimate integral drift ratio was 1/24, showing good resistance capacity against collapse.
- (4) The test specimen had good ductility and energy dissipation capacity. The ultimate ductility coefficient was over 4. The maximum equivalent viscous damping coefficient was over 0.2, which were superior to the reinforced concrete frame with irregular section columns.

Acknowledgments

The authors would like to thank the National Natural Science Foundation of China (Grant No. 50978217), Key Project of Guangxi Natural Science Foundation (Grant No. 2013GXNSFDA019025), Scientific Research Plan Project of Shaanxi Education Department (Grant No. 2013JK0979) of China, and Innovation Group Foundation of Education Ministry of China (Grant No. IRT 13089) and Xi'an University of Architecture and Technology for their generous support of this research work.

References

- Balaji, K.V.G.D. (2001), “Reliability analysis of RC T-shaped column sections”, *Indian Concrete J.*, **75**(3), 223-227.
- Cao, Y.Z., Gan, G. and Tang, J.C. (2007), “Influence of length-width ratio of column limb on aseismic performance of 3D-frames with special-section columns”, *Eng. Mech.*, **24**(4), 118-123.
- Chen, C.C., Li, J.M. and Weng, C.C. (2005), “Experimental behavior and strength of concrete- encased composite beam-columns with T-shaped steel section under cyclic loading”, *J. Construct. Steel Res.*, **61**(7), 863-1006.
- Chen, Z.P., Xue, J.Y. and Zhao, H.T., Shao, Y.J., Zhao, Y.H. and Men, J.J. (2007), “Experimental research on seismic behavior of steel reinforced concrete special-shaped columns”, *J. Build. Struct.*, **28**(3), 53-61.
- Ju, Y.K., Chun, S.C. and Kim, S.D. (2009), “Flexural test of a composite beam using asymmetric steel section with web openings”, *J. Struct. Eng.*, **135**(4), 448-458.
- Karimi, K., El-Dakhkhni, W. and Tait, M. (2012), “Behavior of slender steel-concrete composite columns wrapped with FRP jackets”, *J. Perform. Construct. Facil.*, **26**(5), 590-599.
- Kawano, A., Sakai, J. and Doi, M. (2012), *Damage to Steel Reinforced Concrete Buildings*, Preliminary Reconnaissance Report of the 2011 Tohoku-Chiho Taiheiyo-Okai Earthquake, Springer Japan.
- Kim, S.H., Jung, C.Y. and Ann, J.H. (2011), “Ultimate strength of composite structure with different degrees of shear connection”, *Steel Compos. Struct., Int. J.*, **11**(5), 375-390.
- Lubliner, J. (2006), *Plasticity Theory*, Pearson Education, Upper Saddle River, NJ, USA.
- Ma, H.W., Jiang, W.S. and Cho, C.D. (2011), “Experimental study on two types of new beam-to-column

- connections”, *Steel Compos. Struct., Int. J.*, **11**(4), 291-305.
- Nie, J.G., Xiao, Y. and Chen, L. (2004), “Experimental studies on shear strength of steel-concrete composite beams”, *J. Struct. Eng.*, **130**(8), 1206-1213.
- Pecce, M., Rossi, F. and Bibbò, F.A. and Ceroni, F. (2012), “Experimental behaviour of composite beams subjected to a hogging moment”, *Steel Compos. Struct., Int. J.*, **12**(5), 395-412.
- Tago, S., Teshigawara, M. and Ota, T. (2012), “A seismic evaluation method of medium-high rise steel reinforced concrete buildings for preventing strong collapse”, *J. Japan Assoc. Earthq. Eng.*, **12**(3), 321-333.
- Tsao, W.H. (1993), “A nonlinear computer analysis of biaxially loaded L-shaped slender reinforced concrete columns”, *Comput. Struct.*, **49**(4), 579-588.
- Wang, T.C., Zhang, X.H. and Kang, G.Y. (2007), “Experimental comparison of seismic behavior of two RC frames with specially shaped columns”, *J. Tianjin Univ.*, **40**(7), 791-798.
- Wang, T.C., Zhang, X.H. and Zhao, H.L. (2008), “Experimental study on seismic behavior of RC frames with specially shaped columns reinforced by fiber”, *J. Earthq. Eng. & Eng. Vib.*, **28**(6), 178-185.
- Xue, J.Y., Liu, Y., Zhao, H.T. and Chen, Z.P. (2011), “Experimental study of the bearing capacity of steel reinforced concrete specially-shaped column-beam joint”, *China Civil Eng. J.*, **44**(5), 41-48.
- Yang, T. and Zhang, X.D. (2009), “Research on seismic behavior of frame with T-shaped SRC columns”, *J. Civil, Architect. Environ. Eng.*, **31**(2), 33-37.

CC